On the mechanism of proton-coupled transport by the maltose permease of Saccharomyces cerevisiae

Henderson, Ryan

Chapter 4

Characterization of maltose-binding residues in the central cavity of Mal11

Ryan K. Henderson, Lailatul Nur Ayudya, and Bert Poolman

Manuscript in preparation

Abstract

The proton-coupled symporter Mal11 catalyzes the uptake of maltose into Saccharomyces cerevisiae. Using a predicted structure, we identified eleven likely residues involved in maltose binding or transport in the central cavity of Mal11. We constructed alanine mutants of these amino acids to examine their effects on cellular localization and maltose transport and found critical roles for Asn-249, Trp-252, Gln-256, Gln-379, and Tyr-507. After initial characterization, additional mutations of these five residues were constructed to determine if activity could be restored and found these residues to be largely irreplaceable. Our results suggest a specific sugar-binding site consisting of evolutionarily conserved and unconserved residues, which provides a solid foundation for further studies.

Introduction

The first step of maltose metabolism in yeast is the uptake of the disaccharide across the plasma membrane, which is catalyzed by one of a number of proton-coupled transporters [80,91,116]. One of these, Mal11, is unique in its broad substrate specificity for α-glucosides such as maltose, sucrose, maltotriose, and others [117,118]. Mal11 is a member of the Sugar Porter (SP) family within the Major Facilitator Superfamily (MFS), which consists of sugar transporters that catalyze either downhill facilitated diffusion or uphill substrate transport coupled to the electrochemical proton gradient [37].

Given the importance of sugars as carbon and energy sources, numerous sugar-binding/modifying proteins have been extensively studied, including enzymes, lectins, ligand receptors, substrate-binding proteins, and transporters. Crystal structures of substrate-binding proteins associated with ABC transporters have provided detailed information about the general properties of ligand and sugar recognition. Since the hydroxyl groups of carbohydrates are solvent-exposed and stereospecific, they are often involved in key hydrogen bonds with protein side-chains and thus enable substrate specificity [158]. Indeed, the sugar-binding sites of substrate-binding proteins contain many polar, planar side chains with two or more functional groups capable of forming hydrogen bonds with the sugar hydroxyls [158]. Furthermore, aromatic residues in the binding sites tend to form stacking interactions with monosaccharyl ring units. This is best observed in the maltose or maltodextrin-binding protein (MBP) of *Escherichia coli*, in which the protein forms 16 hydrogen bonds with a bound maltose that is packed between four aromatic residues [159]. In MFS sugar transporters, there is a single substrate-binding site in a central cavity that is formed by the N- and C-halves of the proteins. Just like in other sugar-binding proteins, polar amino acid side chains form hydrogen bonds with the characteristic sugar hydroxyl groups and hydrophobic or aromatic residues stack against the sugar rings. The best characterized is the LacY galactoside transporter from *E. coli*. The binding site residues [17] and the portions of the substrates involved in recognition by the transporter [160] were all but known by the time the first substrate-bound crystal structure was solved [161]. Subsequent structures [162-164] backed up the conclusions from biochemical and biophysical studies that numerous charged and polar residues form hydrogen bonds with the bound substrate and that there is hydrophobic stacking between Trp-151 and one of the galactopyranosyl rings. Similarly, bacterial proton-xylose symporter XylE and the human glucose facilitator GLUT3 are the two SP transporters with ligand-bound structures, and in both cases all hydroxyl groups from the bound sugar form at least one hydrogen bond with the transporter [23,28,165].

While others have explored the energy coupling mechanism of maltose transport in yeast [91,116,117] and we have previously characterized the residues involved in proton-coupling by Mal11 (Chapters 2 and 3), only limited work has been done to examine the sugar binding site of this transporter [166,167]. On the basis of a structural model predicted *de novo* from evolutionary covariation constraints, we identified polar (Asn and Gln) and aromatic (Phe, Trp, Tyr) amino acids in the central cavity of Mal11 and performed mutagenesis to elucidate their roles in the catalytic activity and coupling efficiency of the transporter. These results provide a framework for additional characterization and manipulation of substrate specificity in Mal11.

Materials and Methods

DNA manipulation

All plasmids used in this study are listed in Supplementary Table 1, and all primers in Supplementary Table 2. Mal11 mutants were constructed as described in Chapter 2 by PCR amplification of the *MAL11* gene from pRHA00L [168] as two fragments with 30-40 bp homology at the mutation site using primer 5271 combined with a specific primer for the first fragment and primer 5272 combined with a specific primer for the second fragment. We used primers 5273 and 5274 to amplify the pRHA00L backbone and then used *in vivo* homologous recombination in IMK289 to assemble the three fragments into whole plasmids. To validate strains, plasmids were isolated from transformed IMK289 using a commercial plasmid purification kit (BIOKÉ, Leiden, The Netherlands). The open reading frames of isolated plasmids were sequenced and transformed into *E. coli* for storage.

Strain construction and growth conditions

Saccharomyces cerevisiae strain IMK289 [121], created by replacement of loci *MALx1*, *MALx2*, *MPH2*, and *MPH3* with *loxP* in CEN.PK102-3A (MATa *MALx MAL2x MAL3x leu2-112 ura3-52 MAL2-8*^{C}), was used for Mal11 mutant expression. Synthetic complete drop-out media was made using yeast nitrogen base and a Kaiser leucine drop-out amino acid supplement (Formedium) plus 2 % (w/v) glucose (SD/-Leu) or raffinose (SR/-Leu). For all experiments, yeast cultures were first grown overnight at 30 °C in SD/-Leu, diluted into SR/-Leu, and finally diluted into SR/-Leu plus 0.2 % (w/v) galactose for induction of the *GAL1* promoter during exponential phase of growth. Cells were grown in the presence of galactose for 2.5 h to optimally induce protein expression, at which point they were harvested by centrifugation.

Structural modeling of Mal11

The predicted structure of Mal11 presented in Chapter 2 was used in this study. Briefly, the EVfold server [119,120] was used to perform *de novo* structure prediction of Mal11 based on evolutionary co-variation of residue pairs across a multiple sequence alignment. See Chapter 2 for full details.

Multiple sequence alignment

The primary amino acid sequences of Mal11 homologues were aligned using PSI/TM-Coffee [123] and alignments were visualized using Jalview [124]. Protein sequences were obtained from the following UniProt accession numbers: Mal11 (P54038), Mal21 (E9P8G0), Mal31 (P38156), Mal61 (P15685), Mph2 (P0CD99), XylE (P0AGF4), GLUT1 (P11166), GLUT3 (P11169), bovine GLUT5 (P58353), rat GLUT5 (P43427), and $GlcP_{Se}$ (A0A0H2VG78).

Fluorescence microscopy

Cell pre-growth was executed as described in "Strain construction and growth conditions". Cells induced for Mal11 variant expression were collected by centrifugation at 3,000 g for 5 min at 4 °C, resuspended in 0.1 M potassium phosphate pH 6 or media, and stored on ice until use. Cell samples were placed between a cover slip and a glass slide. A Zeiss LSM

710 scanning confocal microscope (Carl Zeiss MicroImaging, Jena, Germany), equipped with a blue argon laser (488 nm) and a C-Apochromat 40x/1.2 NA objective, was used for fluorescence imaging of live yeast cells expressing Mal11-YPet and mutants. All images were taken with the focal plane at the mid-section of the cells.

Measurement of maltose transport

Yeast cells induced for expression of Mal11 wildtype or mutants were collected by centrifugation at 3,000 g for 5 min at 4 °C, washed twice in assay buffer (10 mM galactose mixed with either 0.1 M potassium-phosphate (KPi) or potassium-citrate phosphate (KCP) buffers) by resuspension in the buffer and repeating centrifugation. Finally, cells were resuspended in assay buffer and kept on ice until use within 4 h. Uphill maltose transport was measured in whole cells at 30 °C. First, cells were incubated for 5-10 min at 30 °C to increase the adenylate energy charge [127]. Next, [U-^{14}C]maltose (600 mCi/mmol; American Radiolabeled Chemicals, Inc.) was added to roughly 48100 Bq/mL to begin the uptake reaction with the maltose concentration ranging from 0.25 mM to 50 mM. At indicated time points, 50 µL samples were taken and mixed with 2 mL ice-cold KPi or KCP buffer, rapidly filtered using cellulose-nitrate filters with 0.45 µm pores (GE-Healthcare, Little Chalfont, UK) that were pre-soaked in KPi or KCP with 1 mM maltose, washed once with another 2 mL KPi or KCP, and finally dissolved in 2 mL scintillation solution (Emulsifier^{plus}, PerkinElmer, Waltham, MA, USA). Radioactivity in each sample was determined by liquid scintillation counting (Tri-Carb 2800TR liquid scintillation analyzer, PerkinElmer). Flow cytometry was used to count the number of cells and determine the fraction of fluorescent cells in the samples. Using this data, the amount of maltose was

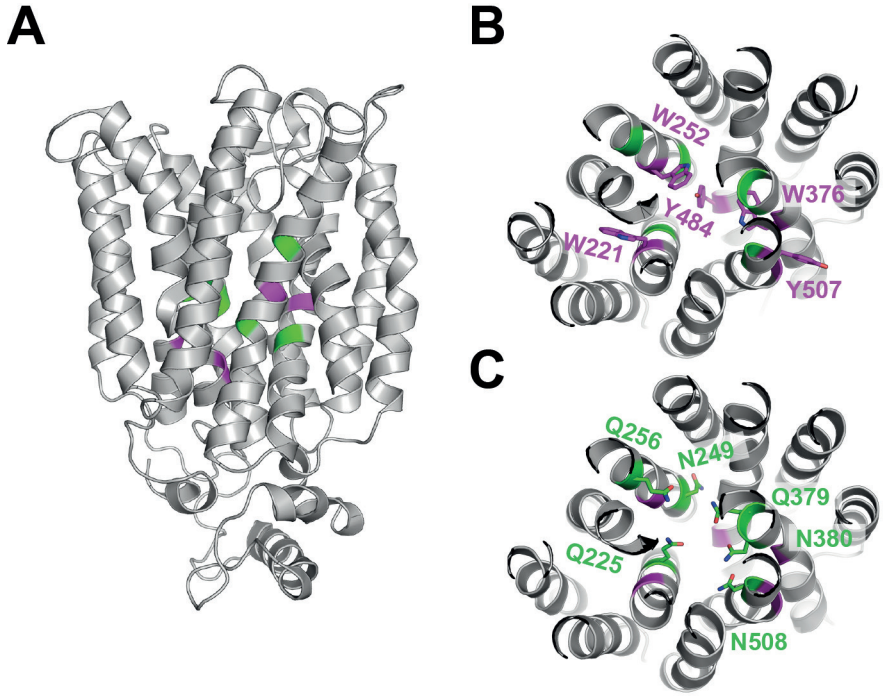

Figure 1. Structural model of potential binding site residues. (A) A side view of the de novo predicted structure of Mal11 using the EVfold server. Aromatic residues of interest are colored magenta (B) and long, polar residues are colored green (C), both shown as a top-view from the extracellular space.

normalized to 10^6 cells and corrected for the fraction of fluorescent cells, that is, the cells expressing Mal11-YPet. We used 60 fL internal volume per cell for intracellular maltose concentration calculations.

Flow cytometry

Samples of cells were diluted to OD_{600} of between 0.25 and 0.4 in assay buffer. We analyzed 20 µL samples with an Accuri C6 flow cytometer (BD Accuri™, Durham, USA), and cellular fluorescence was detected using the flow cytometer's built-in 488 nm laser and FL1 emission detector (533/30 nm).

Results

Identification of possible binding site residues.

Recent crystal structures of sugar transporters with bound substrates have proven essential in understanding general characteristics of sugar recognition [23,28]. Sugars contain polar and nonpolar atoms, and it is thus not surprising that specific binding of the substrate involves a number of polar, nonpolar, and charged residues. Since there is no crystal structure of Mal11 available, we used the EVfold-predicted structural model presented in Chapter 2 (Fig. 1A). This model exhibits the characteristic Major Facilitator Superfamily (MFS) fold in which a central cavity is formed between two domains, each with 6 transmembrane segments (TMs). This central cavity is the single substrate-binding site in all known MFS transporters [37]. We began by examining this region of the protein to select residues with potential roles in sugar binding. We chose to focus on two classes of functionally relevant amino acids: aromatic residues (Phe, Tyr, Trp) and aliphatic, polar residues (Asn, Gln)(Fig. 1B,C). In a multiple sequence alignment of several well-characterized maltose transporters, we found that all of the five aromatic and six polar residues were conserved except for Asn-380 (Fig. 2).

Comparison of Mal11 with sugar transporters with known structures

We used a multiple sequence alignment to compare the identified residues in Mal11 with a number of SP transporters with known structures: XylE from *E. coli*, GLUT1 and GLUT3 from *H. sapiens*, GLUT5 from *R. norvegicus* (rGLUT5) and *B. taurus* (bGLUT5), and GlcP$_{Se}$ from *S. epidermidis* (Fig. 3). These monosaccharide transporters are members of the Sugar Porter (SP) family within the MFS and have high sequence conservation with each other, whereas Mal11 is more distantly related. We found that residues Asn-249 and Glu-379 are very similar or invariant across these sequences, indicating critical roles in sugar binding/transport. Furthermore, Trp-252, Glu-256, Asn-380, Tyr-484, Tyr-507, and Asn-508 align to substrate-binding positions in the homologues, indicating potential roles for those in Mal11 as well. Finally, Trp-221, Gln-225, and Trp-376 are not conserved in the monosaccharide transporters and do not align to known substrate-binding residues. Since Mal11 has different specificity and transports disaccharides, these three could still be involved in sugar binding.

Characterization of alanine mutants

We substituted each of the 11 identified residues for alanine and transformed the multicopy plasmids containing YPet-tagged mutant transporters into IMK289. This back-

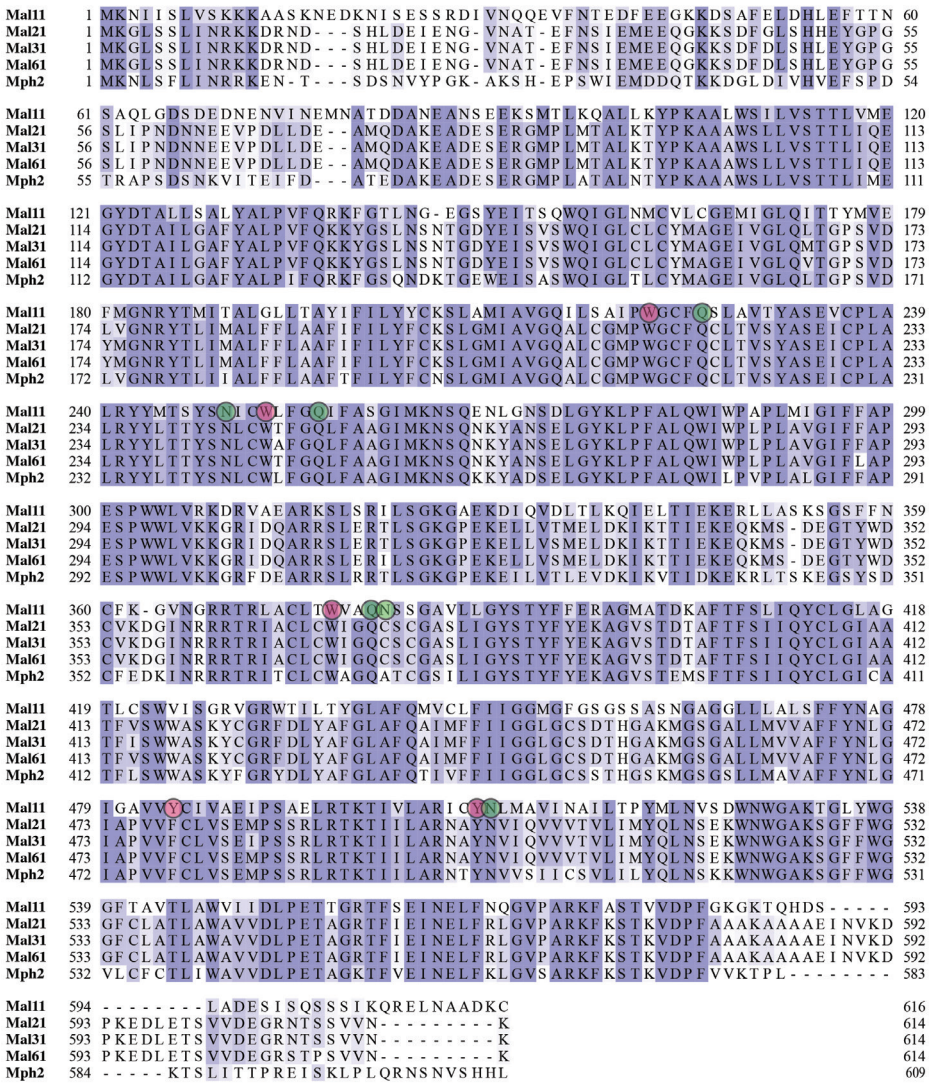

Figure 2. Multiple sequence alignment of maltose transporters. Comparison of the primary sequences of five closely-related maltose and α-glucoside transporters from *S. cerevisiae*: Mal11, Mal21, Mal31, Mal61, and Mph2. The sequences are highlighted blue to show conservation calculated using the BLOSUM62 substitution matrix. Potential binding-site residues of Mal11 are in green (long, polar residues) or magenta (aromatic residues) circles.

ground strain contains no enzymes involved in α-glucoside transport or catabolism, and thus the observed activity can only be from the expressed mutant proteins [121]. We used a similar mutant-screening pipeline to what is described in Chapter 2; we first examined cellular localization of the YPet-tagged mutants using fluorescence microscopy, followed by measurement of radiolabelled maltose uptake into whole cells. We found that 10 of the 11 alanine mutants localized predominantly to the plasma membrane (Fig. 4A), although Q256A and N380A both show significant fluorescence in subcellular compartments. The

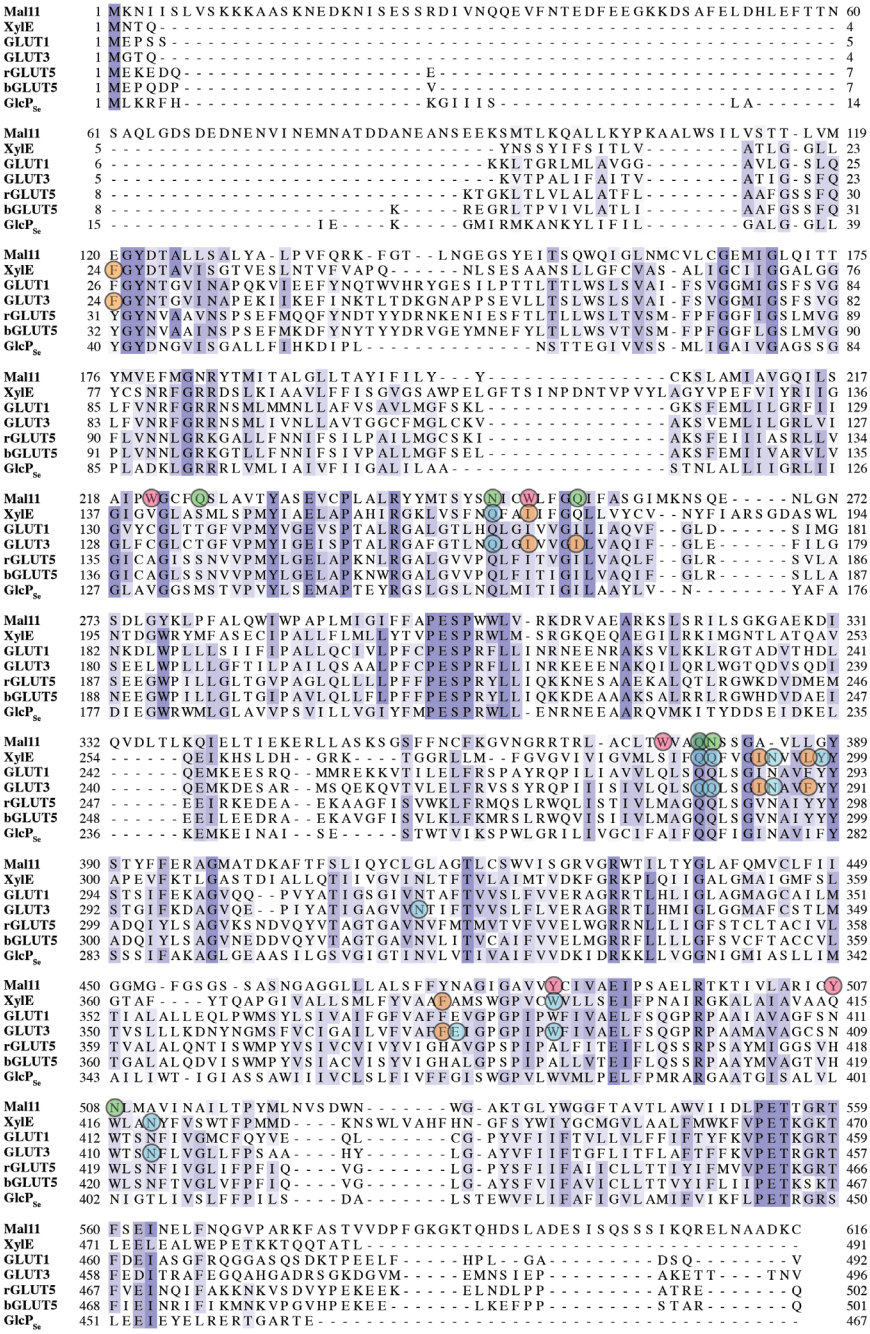

Figure 3: Multiple sequence alignment of Sugar Porter members. Comparison of the primary sequences of Mal11 with six Sugar Porters with known structures: XylE, GLUT1, GLUT3, rat GLUT5, bovine GLUT5, and GlcPSe. Like in Figure 2, conservation is shown using blue highlighting and calculated with the BLOSUM62 substitution matrix. The potential binding site residues of Mal11 are circled in green (long, polar residues) and magenta (aromatic residues). For XylE and GLUT3, for which ligand-bound structures have been solved, residues that hydrogen bond (cyan) or have van der Waals interactions (orange) with the ligand (xylose for XylE, glucose for GLUT3) are circled.

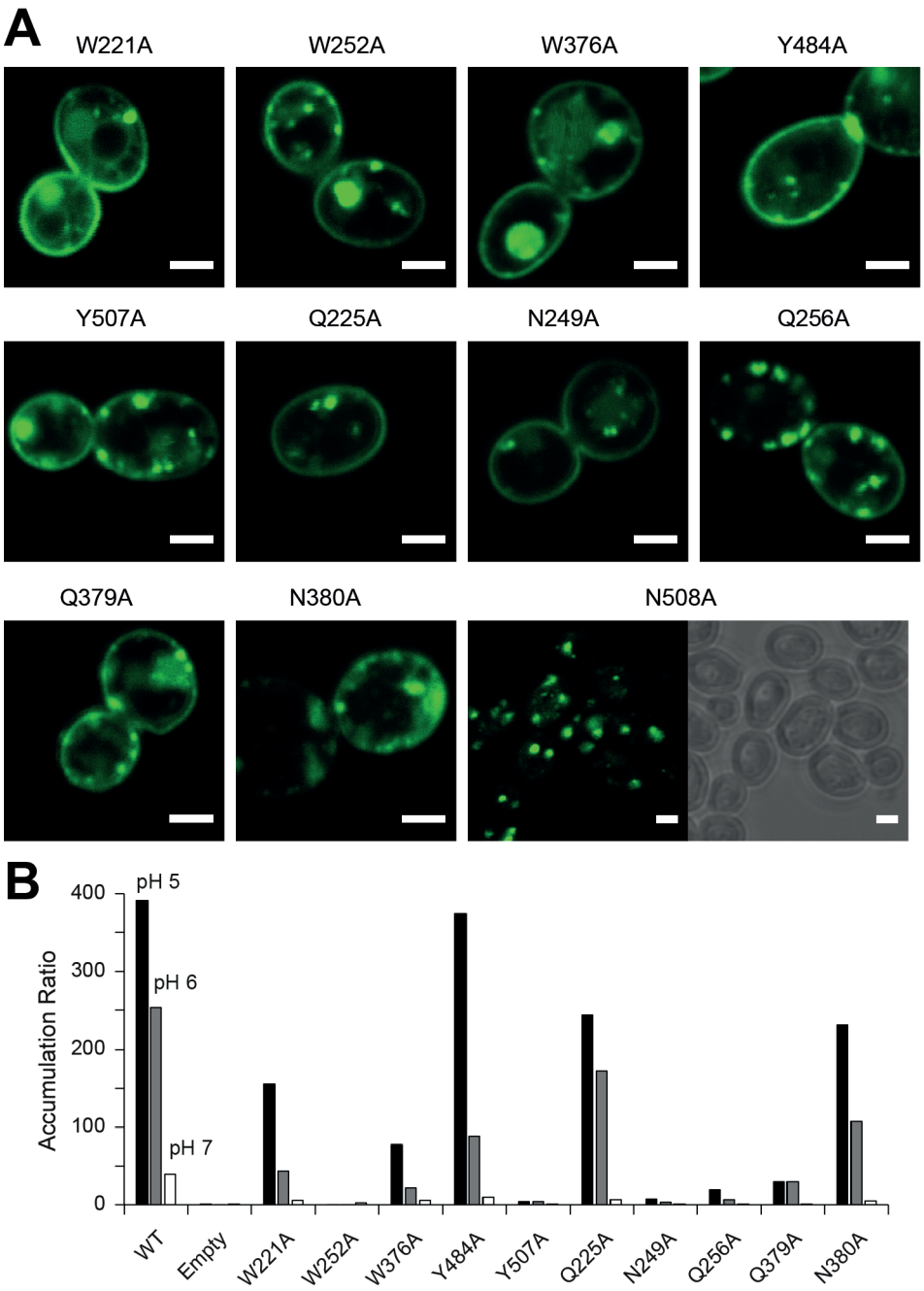

Figure 4: Characterization of alanine mutants. (A) Representative confocal fluorescence microscopy images of IMK289 cells expressing alanine mutants of Mal11-YPet from the *GAL1* promoter after 2.5 h of galactose induction. Scale bars represent 2 µm. (B) Uphill maltose transport by IMK289 cells expressing alanine mutants of Mal11-YPet in K-citrate phosphate at pH 5 (black columns) and pH 7 (white columns), or K-phosphate pH 6 (grey columns). Cells were diluted to an OD_{600} of 4 and incubated with 1 mM [U-^{14}C]maltose at 30 °C for at least 50 min, and the final accumulation ratios of maltose are indicated as columns.

eleventh, N508A, exhibited intracellular localization, most likely to the cortical endoplasmic reticulum and vacuole. Interestingly, Asn-508 is located one helix turn above Arg-504, the alanine mutant of which also causes improper localization and may be involved in a salt bridge that helps to govern proton coupling in the transporter, as discussed in Chapter 3.

Next, we measured transport of maltose at pH 6 by the mutants with proper localization (Fig. 4B). Two of the mutants, W252A and Y507A, displayed no transport, while another three (N249A, Q256A, and Q379A) had less than 10% activity compared to wildtype Mal11. All five of these are situated in conserved sugar-binding positions, with Asn-249 and Gln-379 highly conserved in the SP family (Fig. 2). W376A also had severely di-

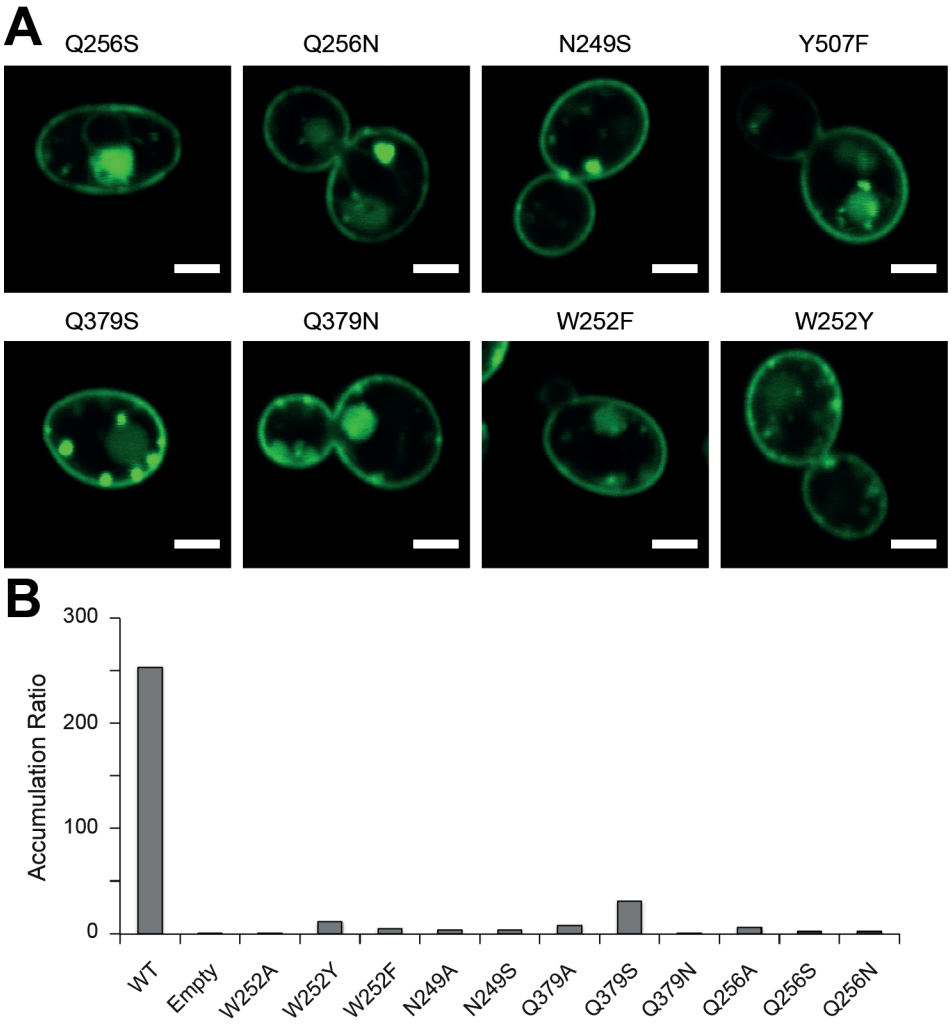

Figure 5: Characterization of additional Mal11 mutants. (A) Representative fluorescence microscopy images of IMK289 cells expressing mutants of Mal11-YPet from the *GAL1* promoter after 2.5 h of galactose induction. Scale bars represent 2 μm. (B) Uphill maltose transport by IMK289 cells expressing mutants of Mal11-YPet. Cells were diluted in K-phosphate pH 6 to an OD_{600} of 4 and incubated with 1 mM [U-^{14}C]maltose at 30 °C for at least 50 min. Columns indicate the final accumulation ratios.

minished sugar transport with ~20% the wildtype activity, while the remaining mutants maintained significant maltose transport. We have previously observed altered pH-dependence of sugar transport upon mutagenesis of key residues, such as for mutants of Glu-167 (Chapter 2). Therefore, we then compared maltose transport by mutants with detectable activity at pH 5 and pH 7 (Fig. 4B). Contrary to what was observed in mutants of Glu-167, the mutants of putative binding-site residues showed similar profiles of pH-dependent uptake as wildtype Mal11.

Additional mutagenesis of irreplaceable residues

We further investigated the roles of the five residues whose alanine mutants have less than 10% transport activity compared to wildtype Mal11 by constructing additional mutants. We observed proper plasma membrane localization for each of the new mutant transporters (Fig. 5A). Next, we measured maltose uptake by these transporters and found that while W252A and Y507A were fully inactive, mutants W252Y and Y507F retained a small but significant transport activity; W252F was also inactive (Fig. 5B). This indicates that there should be a residue with some polarity at position 252 and an aromatic residue at 507. Additionally, activity was abolished in mutants N249S, Q256S, Q256N, and Q379N, indicating that the wildtype residues are greatly preferred even when the mutated residue has a side-chain with similar properties as the genuine amino acid. The effect of pH on transport by these mutants was similar to what was observed in the alanine mutants in that transport was high at pH 5 and decreased with increasing pH (Fig. 6).

Dependence of transport on sugar concentration

We then measured the initial transport rate as a function of maltose concentration and were able to estimate kinetic parameters K_m and V_{max} for mutants Y484A and W252Y (Fig. 7). The K_m values for the mutants were higher (i.e. lower transport affinity) than for the wildtype transporter, indicating some role for these residues in maltose binding. Notably, W252Y showed a roughly ten-fold increase in K_m. Surprisingly, there was not a large decrease in V_{max} for these mutants. For the other mutants tested (Q225A, N249A, N380A,

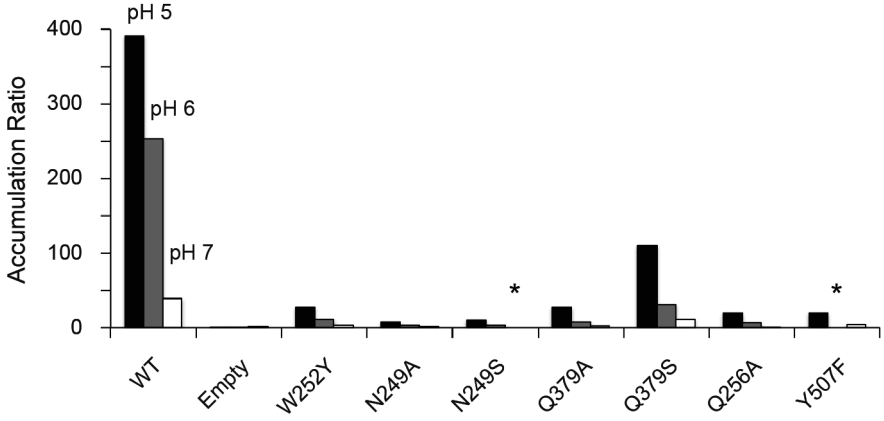

Figure 6: pH-dependence of maltose uptake. Uphill maltose transport by IMK289 cells expressing mutants of Mal11-YPet in K-citrate phosphate at pH 5 (black columns) and pH 7 (white columns), or K-phosphate pH 6 (grey columns). Cells were diluted to an OD_{600} of 4 and incubated with 1 mM [U-^{14}C]maltose at 30 °C for at least 50 min, and the final accumulation ratios of maltose are indicated as columns. The asterisks indicate that no data is shown for N249S at pH 7 or for Y507F at pH 6.

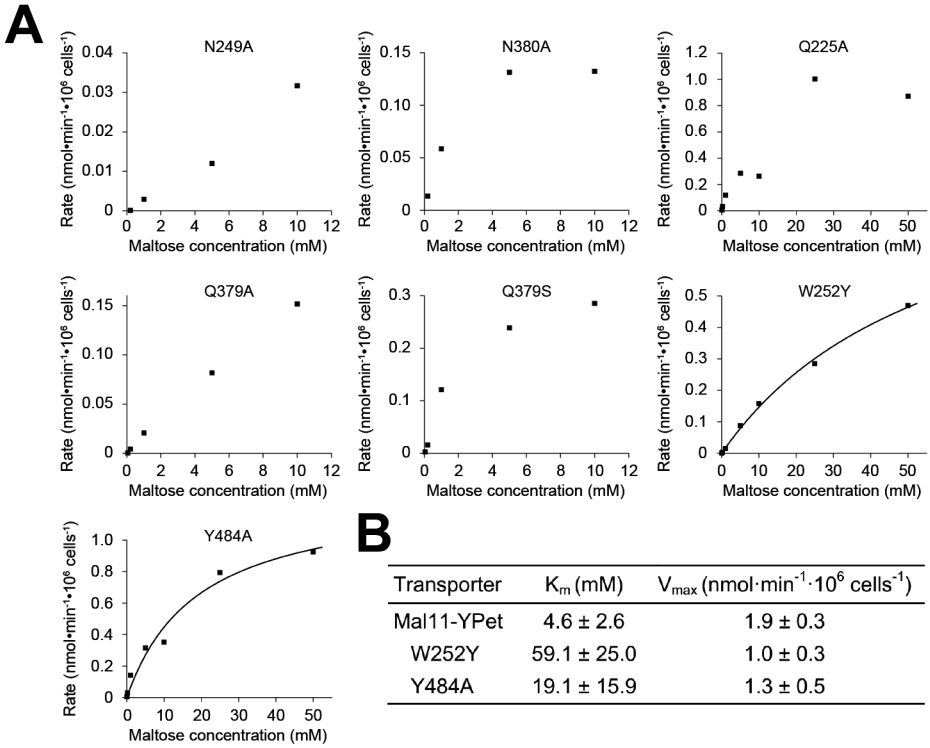

B

Transporter	K_m (mM)	V_{max} (nmol·min^{-1}·10^6 cells^{-1})
Mal11-YPet	4.6 ± 2.6	1.9 ± 0.3
W252Y	59.1 ± 25.0	1.0 ± 0.3
Y484A	19.1 ± 15.9	1.3 ± 0.5

Figure 7: Dependence of transport rate on maltose concentration. (A) Plots of substrate concentration versus initial transport rate for Mal11-YPet and seven mutant transporters. The calculated K_m and V_{max} values of those with sufficient data are shown. Transport was measured at concentrations ranging from 0.25 mM to 50 mM [U-^{14}C]maltose at 30 °C, and the initial rate was calculated from the linear part of the transport curve. (B) Michaelis-Menten kinetic parameters were estimated for W252Y and Y484A. The values for wildtype Mal11-YPet are taken from Chapter 2.

Q379A, and Q379S), the activity at high maltose concentrations was too low or the error too high to accurately estimate a K_m and V_{max}.

Discussion

We have used mutagenesis to demonstrate the necessity of eleven aromatic and polar amino acids located in the central cavity of the transporter. Of the residues examined, the alanine mutants of five showed little or no activity: Asn-249, Trp-252, Gln-256, Gln-379, and Tyr-507 (Fig. 4B). Mutants W252A and Y507A showed no transport activity at all. This most likely occurs due to a strong reduction in maltose binding affinity, although an alternative explanation would be that these residues stabilize the transporter in one conformation such that transport cannot occur. Localization of YPet-tagged protein was used in this study to screen for improperly-folded/targeted transporters, but inactivity due to locking of the protein in an outward or inward-facing conformation may not affect the localization, as has been observed in the yeast arginine transporter Can1 [169]. Asn-249 and Gln-379 are highly conserved in homologous transporters (Fig. 2, 3) and mutations at the corresponding sites in XylE and GLUT1 cause significant reductions in transport [23,170,171]. Interestingly, it has been shown that mutation of Gln-166 in rGLUT5 (Asn-

249 in Mal11) to glutamic acid causes a shift in substrate specificity from fructose to glucose [29]. Although we observed little maltose transport by mutants N249A and N249S, it would be useful to perform further tests to see if a similar change in transported substrate can be observed. The other three residues (Trp-252, Gln-256, Tyr-507) are not conserved in the bacterial and human homologues, but are fully conserved among the maltose transporter homologues from yeast (Fig. 2,3).

Mutations to a number of residues had smaller effects on substrate transport Tyr-484 is special because the homologous residue in XylE, GLUT1, and GLUT3 closes the bottom of the central cavity [23,26,28], and mutation to alanine in XylE (Trp-392) almost fully abrogates all transport and counterflow activity [23]. Interestingly, this is not the case for rGLUT5 or bGLUT5, both of which have a deeper central cavity due to the presence of alanine at this position [29]. Because we observed only a slight reduction in activity upon mutation to alanine, Tyr-484 does not appear to have a significant contribution to substrate binding/transport (Fig. 4B). Alternatively, a deeper central cavity may change how maltose binds to the transporter but not the rate of transport. If the substrate binds deeper in the cavity, then the substrate specificity of Mal11-Y484A is expected to be different. Further studies will be needed to test this.

In Chapter 2, we demonstrated that neutral mutants of acidic residues generally do not affect the K_m for maltose transport by Mal11 with the exception of E120Q, which increased the K_m ten-fold. While this position is a conserved substrate-binding residue, it is generally aromatic in distant SP homologues (Fig. 2,3). We know from our work in Chapter 2 that Glu-120 is involved with proton coupling. Residues Trp-221, Gln-225, and Trp-376 are conserved in the maltose transporters but not in more distant SP transporters, and their alanine mutations had minor or moderate effects on transport activity of Mal11 (Fig. 2,3,4B). These three residues are in close proximity to Arg-504 and Glu-167, which likely form a salt bridge involved in mediating proton coupling and are also not conserved in more distant SP transporters. This suggests that Trp-221, Gln-225, and Trp-376 have evolved to take part in the complex interactions necessary for regulating proton coupling, perhaps by creating an environment around this salt bridge to make such an interaction more favorable, and therefore these residues are not crucially involved in sugar binding. In fact, we show in Chapter 3 that mutation of Trp-376 to serine restores transport activity to the uncoupled mutant Mal11-E120A/D123N/E167A. Additionally, we found that mutating Asn-508 to alanine caused improper localization of the transporter (Fig. 4A). This residue is also not conserved in the more distant SP transporters but is invariant in maltose transporter homologues, and we hypothesize that this residue also serves to accommodate the possible salt bridge between Arg-504 and Glu-167. Since it is located at the interface between the N- and C-halves of Mal11, Asn-508 may have additional roles in protein stability and conformational regulation, and therefore mutation of it leads to mislocalization.

A number of central cavity residues are known binding site residues in the bacterial and mammalian SP homologues but are not conserved in the maltose transporters and may be involved in the diverse substrate specificities observed between members of the family. A conserved tyrosine in TM7 of XylE (Tyr-298) and the GLUT transporters is purportedly involved in closing off the sugar-binding site from the bulk water of the extracellular space [27,37]. In maltose transporter homologues, Gly-388 occupies this position and there is

instead a tyrosine located one helix turn above it (Tyr-392). Additionally, maltose is an exofacial competitive inhibitor of glucose transport by GLUT3, and in the structure of the maltose-bound transporter this tyrosine is oriented away from the central cavity, implying that the binding site is unable to be closed off from the extracellular space, which may provide a structural basis for the inhibition [28]. Therefore, we suggest that the location of the tyrosine in this helix may in part sterically dictate the size of the saccharide that can be transported by the protein. It is then possible that the substrate specificity of Mal11 could be limited to only monosaccharides by making a double mutation to Mal11 (G388Y and A384N) to make it more similar to XylE and the GLUT transporters.

There are a number of unanswered questions that should be addressed in future work. Given the industrial relevance of maltose, maltotriose, and trehalose as feedstocks, the molecular basis of substrate specificities within the maltose transporter families is of great importance. Analysis of the variation in substrate-binding and central cavity residues among these transporters should be performed to identify which residues are responsible for the various substrate specificities. This then leads to another question for the future: can we design binding sites for specific sugars (or other substrates), and what are the limitations to the substrates Mal11 can transport? The MFS members are known for transporting a vast diversity of substrates, including amino acids, sugars, ions, and drugs [6], and comparing substrate-binding strategies among MFS transporters will help us to fully understand the molecular basis of transport by this important superfamily.

Acknowledgements

This work was carried out within the BE-Basic R&D Program, which was granted a FES subsidy from the Dutch Ministry of Economic affairs, agriculture and innovation (EL&I). The research was also funded by a NWO TOP- PUNT (project number 13.006) grant.

Supplementary Information

Supplementary Table 1. Plasmids used in this study

Plasmid	Description	Reference
pFB001	pRS426GAL1-GFP derivative, *lyp1-TEV-YPet-his*	[57]
pRHA00L	pFB001 derivative with *LEU2* and *MAL11-TEV-YPet-his*	Chapter 2
pR200	pRHA00L derivative with MAL11-W221A	This study
pR201	pRHA00L derivative with MAL11-W252A	This study
pR202	pRHA00L derivative with MAL11-W376A	This study
pR203	pRHA00L derivative with MAL11-Y484A	This study
pR204	pRHA00L derivative with MAL11-Y507A	This study
pR205	pRHA00L derivative with MAL11-Q225A	This study
pR206	pRHA00L derivative with MAL11-N249A	This study
pR207	pRHA00L derivative with MAL11-Q256A	This study
pR208	pRHA00L derivative with MAL11-Q379A	This study
pR209	pRHA00L derivative with MAL11-N380A	This study
pR210	pRHA00L derivative with MAL11-N508A	This study
pR211	pRHA00L derivative with MAL11-N249S	This study
pR212	pRHA00L derivative with MAL11-W252Y	This study
pR213	pRHA00L derivative with MAL11-W252F	This study
pR214	pRHA00L derivative with MAL11-Q256S	This study
pR215	pRHA00L derivative with MAL11-Q256N	This study
pR216	pRHA00L derivative with MAL11-Q379S	This study
pR217	pRHA00L derivative with MAL11-Q379N	This study
pR218	pRHA00L derivative with MAL11-Y507F	This study

Supplementary Table 2. Primers used in this study

Primer name	Sequence (5' to 3')	Description
5271	CAAGGAGAAAAAACCCCGGATTCTAGAACTAG TGGATCCCCCATGAAAAATATCATTTCATTGGT AAG	Fw primer for homologous recombination of Mal11 into pFB001
5272	GAATAATTCTTCACCTTTAGAACCTTGAAAATA TAAATTTTCCCCTCCACATTTATCAGCTGCATT TAATTC	Rev primer for homologous recombination of Mal11 into pFB001
5273	GGAGGGGAAAATTTATATTTTCAAGGTTC	Fw primer for linearizing pFB001
5274	GGGGGATCCACTAGTTCTAGAATC	Rev primer for linearizing pFB001
6550	TTCTCTCAGCTATACCAGCTGGTTGTTTCCAAA GTTTGG	W221A mutagenesis
6551	AACAGCCAAACTTTGGAAACAACCAGCTGGTA TAGCTGAGAG	W221A mutagenesis
6552	AGTTACTCCAACATTTGTGCTTTATTTGGTCAA ATCTTCGC	W252A mutagenesis
6553	AAGATTTGACCAAATAAAGCACAAATGTTGGA GTAACTGG	W252A mutagenesis
6554	AGACTTGCATGTTTAACTGCTGTAGCTCAAAAT AGTAGC	W376A mutagenesis
6555	TACTATTTTGAGCTACAGCAGTTAAACATGCAA GTCTCG	W376A mutagenesis
6556	TGGTATCGGTGCAGTTGTTGCTTGTATCGTTGC TG	Y484A mutagenesis
6557	TTCAGCAACGATACAAGCAACAACTGCACCGA TACC	Y484A mutagenesis
6558	TAGTGCTGGCCCGTATTTGCGCTAATCTCATGG	Y507A mutagenesis
6559	TAACGGCCATGAGATTAGCGCAAATACGGGCC AGC	Y507A mutagenesis
6560	ATACCATGGGGTTGTTTCGCTAGTTTGGCTGTT ACTTATGC	Q225A mutagenesis
6561	AAGTAACAGCCAAACTAGCGAAACAACCCCAT GGTATAGC	Q225A mutagenesis
6562	ACATGACCAGTTACTCCGCTATTTGTTGGTTAT TTGG	N249A mutagenesis
6563	TGACCAAATAACCAACAAATAGCGGAGTAACT GGTCATG	N249A mutagenesis
6564	AACATTTGTTGGTTATTTGGTGCTATCTTCGCC TCTGG	Q256A mutagenesis
6565	TACCAGAGGCGAAGATAGCACCAAATAACCAA CAAATGTTGG	Q256A mutagenesis
6566	TTGCATGTTTAACTTGGGTAGCTGCTAATAGTA GCGG	Q379A mutagenesis
6567	AACGGCACCGCTACTATTAGCAGCTACCCAAG TTAAACATG	Q379A mutagenesis
6568	ATGTTTAACTTGGGTAGCTCAAGCTAGTAGCG GTGC	N380A mutagenesis
6569	AAACGGCACCGCTACTAGCTTGAGCTACCCAA G	N380A mutagenesis
6570	TGGCCCGTATTTGCTACGCTCTCATGGCCGTTA TTAACG	N508A mutagenesis
6571	TAACGGCCATGAGAGCGTAGCAAATACGGGCC AGCAC	N508A mutagenesis
6817	ACATGACCAGTTACTCCTCTATTTGTTGGTTAT TTGG	N249S mutagenesis
6818	TGACCAAATAACCAACAAATAGAGGAGTAACT GGTCATG	N249S mutagenesis
6819	AGTTACTCCAACATTTGTTATTTATTTGGTCAA ATCTTCGC	W252Y mutagenesis
6820	AAGATTTGACCAAATAAATAACAAATGTTGGA GTAACTGG	W252Y mutagenesis
6821	AGTTACTCCAACATTTGTTTTTTATTTGGTCAA ATCTTCGC	W252F mutagenesis
6822	AAGATTTGACCAAATAAAAAACAAATGTTGGA GTAACTGG	W252F mutagenesis
6823	AACATTTGTTGGTTATTTGGTTCTATCTTCGCCT CTGG	Q256S mutagenesis
6824	TACCAGAGGCGAAGATAGAACCAAATAACCAA CAAATGTTGG	Q256S mutagenesis
6825	AACATTTGTTGGTTATTTGGTAATATCTTCGCC TCTGG	Q256N mutagenesis
6826	TACCAGAGGCGAAGATATTACCAAATAACCAA CAAATGTTGG	Q256N mutagenesis
6827	TTGCATGTTTAACTTGGGTAGCTTCTAATAGTA GCGG	Q379S mutagenesis
6828	AACGGCACCGCTACTATTAGAAGCTACCCAAG TTAAACATG	Q379S mutagenesis
6829	TTGCATGTTTAACTTGGGTAGCTAATAATAGTA GCGG	Q379N mutagenesis
6830	AACGGCACCGCTACTATTATTAGCTACCCAAGT TAAACATG	Q379N mutagenesis
6831	TAGTGCTGGCCCGTATTTGCTTTAATCTCATGG	Y507F mutagenesis
6832	TAACGGCCATGAGATTAAAGCAAATACGGGCC AGC	Y507F mutagenesis